Acoustic liners for jet-installation noise reduction

Original
Acoustic liners for jet-installation noise reduction / Rego, L., Avallone, F., Ragni, D., Casalino, D., Denayer, H.. - In: JOURNAL OF SOUND AND VIBRATION. - ISSN 0022-460X. - 537:(2022), p. 117189. [10.1016/j.jsv.2022.117189]

Publisher:
Elsevier

Published
DOI:10.1016/j.jsv.2022.117189

Journal of Sound and Vibration 537 (2022) 117189

Contents lists available at ScienceDirect

Journal of Sound and Vibration

journal homepage: www.elsevier.com/locate/jsvi

Acoustic liners for jet-installation noise reduction

Leandro Rego [a,*], Francesco Avallone [a], Daniele Ragni [a], Damiano Casalino [a], Hervé Denayer [b,c]

[a] *Delft University of Technology, Department of Aerodynamics, Wind Energy and Propulsion, Kluyverweg 1, 2629 HS Delft, The Netherlands*
[b] *KU Leuven, Department of Mechanical Engineering, Celestijnenlaan 300B, 3001 Leuven, Belgium*
[c] *Flanders Make – DMMS Core Lab, Belgium*

ARTICLE INFO

Keywords:
Aeroacoustics
Jet-installation noise
Acoustic liners
Helmholtz resonators

ABSTRACT

A Helmholtz resonator with a curved cavity is studied for reducing jet-installation noise in a configuration comprised by a subsonic jet and a nearby flat plate. The face-sheet and cavity are designed with the Guess method and the impedance is verified through an experiment and a simulation of an impedance tube. Both single and double degree-of-freedom liners, the latter with a perforated septum inside the cavity, are studied. A good agreement is obtained for the impedance curves from the design method and the experimental and numerical impedance tube, particularly at frequencies close to the absorption peak. Numerical simulations of the installed jet are performed with an array of resonators placed inside the plate with the face-sheet on the lower side, targeting noise reduction at a ground observer. Far-field spectra show that noise reduction in the order of 7 dB is obtained with respect to the baseline solid plate, at the resonance frequency of the single degree-of-freedom liner. Moreover, there is a broad frequency range around the resonance in which the sound pressure levels of the lined plate are lower. For the configuration with the double degree-of-freedom resonator, further noise reduction (approximately 3 dB) is obtained at higher frequencies, around the second peak in the absorption coefficient curve. The results also show that a slight noise reduction (2 - 3 dB) occurs for an observer on the shielded side of the plate, but in a significantly narrower band around the resonance frequency. This is attributed to the absorption of acoustic waves from the jet itself prior to their scattering at the trailing edge, coupled with a less abrupt impedance discontinuity at the trailing edge. Consequently, the resonators also act by reducing the strength of the acoustic source at the designed resonance frequency.

1. Introduction

The progressive increase of bypass ratio in aircraft turbofan engines has led to significant jet noise reduction [1]. However, the consequent larger engine diameter results in an interaction between the exhaust jet and nearby airframe surfaces, producing an acoustic source known as Jet-Installation Noise (JIN) [2–4]. This source arises at the wing trailing edge due to scattering of hydrodynamic pressure waves generated in the jet mixing layer as sound to the far-field [5]. The main noise increase is broadband in nature and it occurs at low and mid frequencies, particularly in the directions normal and upstream of the jet axis [6,7]. Installation effects are also responsible for reflection of acoustic waves generated by quadrupole sources in the jet plume [3] and acoustic shielding on the opposite side of the surface [8]. Recent computational results of aircraft acoustic footprint have shown that installation effects are responsible for penalties of approximately 4 EPNdB at full aircraft level [9]. In the near future, with the

---

[*] Corresponding author.
E-mail address: l.rego@tudelft.nl (L. Rego).

https://doi.org/10.1016/j.jsv.2022.117189
Received 20 September 2021; Received in revised form 31 May 2022; Accepted 12 July 2022

development of ultra-high bypass ratio engines, this source will likely become more dominant due to increased proximity between engine and airframe [10]. Therefore, the development of noise reduction solutions for this particular source is of interest.

A solution for JIN reduction is the application of flow-permeable materials on the scattering surface. Through measurements with a flat plate placed in the vicinity of a single-stream jet, Rego et al. [11] have shown that noise reduction in the order of 9 dB at the spectral peak is achieved by replacing the solid trailing edge of the surface with a metal foam. Moreover, Rego et al. [12] have linked this result to the near-field characteristics of the flow, such as a better pressure balance between the upper and lower sides of the plate and a reduction in the spanwise pressure coherence at the plate trailing edge. They have also shown that the amplitude of noise reduction is connected to the properties of the permeable material such as porosity and resistivity, up to a certain threshold [12]. However, for a partially porous surface, scattering still occurs at the solid-permeable junction, which becomes the location of the dominant acoustic source at the plate [12]. On the other hand, having a fully permeable surface without junction effects is unfeasible since that would lead to degradation of aerodynamic characteristics, i.e. lift decrease and drag increase [13,14].

A different noise reduction solution, with a potential application for JIN, is the acoustic liner. This concept is based on an array of Helmholtz resonators, comprising a porous face-sheet, a cavity and a solid backplate, which is also known as a Single Degree-of-Freedom (SDOF) liner. When the incident acoustic waves have low Sound Pressure Level (SPL), the working principle of a liner is mainly to dampen noise through thermal and viscous losses within the orifices in the face-sheet. Additionally, for high SPL, acoustic energy is converted into vorticity by vortex shedding at the edges of the orifices [15,16]. Liners are usually effective acoustic treatments in a narrow frequency band, but, under certain conditions, they can provide noise mitigation in a sufficiently broad range. This happens, for example, with high-amplitude incident sound waves, for which the liner presents a non-linear behavior. Under these conditions, vortex shedding occurs at the openings of the face-sheet and the frequency range of reduction is a function of the Reynolds number at the orifice [16,17]. Moreover, the addition of a porous septum inside the cavity (Double Degree-of-Freedom - DDOF liner) results in a second absorption peak and a broader frequency range of noise dampening [18]. Since JIN is a broadband source, it is necessary that resonators designed for this application provide sound absorption in a sufficiently broad range of wavelengths.

Liner technology has been already studied for noise reduction of aircraft broadband sources. Casalino and Barbarino [19] have developed a lined flap concept, for which the whole flap is conceived as a liner composite structure. The goal of this treatment is to attenuate turbulent boundary-layer trailing-edge noise and tip vortex noise, which are inherently broadband sources [19]. Both SDOF and DDOF configurations with the porous face-sheet on the lower side of the flap have been analyzed through a combination of a numerical CFD solution and a finite-element method for the acoustic propagation. The lined flap provides noise reduction in the order of 6.4 dB with respect to the baseline case, thus confirming that a lined airframe structure is effective in reducing noise of broadband characteristic [19].

Based on these results, it is believed that acoustic liners are a potential JIN reduction solution, when applied at the surface close to the jet. In comparison to open-cell permeable materials, the resonators only have open channels on the face-sheet, but the backplate is fully solid. Therefore, since there is no flow communication between the two sides of the airframe surface, deterioration of its aerodynamic characteristics can be minimized [20]. As a consequence, the whole surface can be treated with liners, instead of having it restricted to the trailing-edge region, thus also avoiding junction scattering effects [11,21]. Therefore, by carefully choosing the geometry and dimensions of the resonator, it is believed that this technology can be feasibly applied for JIN reduction.

Since JIN is dominant at low frequencies, the theory states that long cavities are required to achieve noise reduction [22]. Therefore, since they have to be mounted in a relatively thin surface, a curved resonator concept is adopted for this work, for which the cavity curves to a direction parallel to the face-sheet. This type of resonator has been already investigated, particularly for low-frequency noise attenuation [23,24]. Sugimoto, Murray and Astley [25], for example, have shown through finite element analyses that an L-shaped resonator is effective for attenuating noise of a modeled source at different frequencies, and its properties can be tuned similarly to regular resonator concepts [25]. However, it is possible that the liners may also alter the source behavior, which has not yet been demonstrated.

Therefore, this work studies a curved resonator concept for JIN mitigation in an installed jet set-up comprised by a flat plate and a single-stream jet, as well as the underlying mechanisms behind the noise reduction. For the chosen configurations, there is no grazing flow on the surface and the only addressed noise generation mechanism is the scattering of evanescent waves at the plate trailing edge. The face-sheet and cavity are designed with the method proposed by Guess [26] and the impedance is verified through an experiment and simulations of an impedance tube. Both SDOF and DDOF liners are investigated. Numerical simulations of the installed jet are then performed with the resonators placed in the plate and the results are compared with the baseline solid configuration. The simulations are performed using a lattice-Boltzmann solver coupled with a Very Large Eddy Simulation model (LBM-VLES). This method has been chosen since it can resolve the flow field with a relatively low computational cost, still showing very good agreement with experimental data [7]. Additionally, the effect of the impingement of evanescent waves from the jet hydrodynamic field on the lined plate, as well as potential modifications to the source properties by the resonators can be verified. The baseline installed jet configuration investigated in this paper replicates the one from Rego et al. [27].

This paper is organized as follows. In Section 2, the methodology is reported, including descriptions of the design equations for the resonators, the impedance characterization, the flow solver and the chosen installed jet test case. Section 3 contains the design of the resonator and validation of its properties. In Section 4, the results for the installed jet with a lined plate are discussed, focusing on the far-field behavior and source characteristics. Finally, the most important findings of this work are summarized in the conclusions.

2. Methodology

2.1. Resonator design

The design of the SDOF resonator for JIN reduction follows the method described by Guess [26], which is valid for Helmholtz resonators constituted by a perforated face-sheet, a cavity and a solid backplate. This method is based on the concept of acoustic impedance z, in terms of resistance θ and reactance χ, as given by [26]:

$$z = \theta + \mathrm{i}\chi. \tag{1}$$

All parameters in this equation are non-dimensionalized by the characteristic impedance of the fluid ρc_0, where ρ is the density and c_0 is the speed of sound. The expression for the resistance is given by [26]:

$$\theta = \frac{\sqrt{8\nu\omega}}{\sigma c_0}\left(1+\frac{t}{d}\right) + \frac{\pi^2}{2\sigma}\left(\frac{d}{\lambda}\right)^2 + \frac{(1-\sigma^2)}{\sigma}\left[\frac{|u_0|}{c_0} + kM\right], \tag{2}$$

where ν is the fluid kinematic viscosity, ω is the angular frequency ($\omega = 2\pi f$), σ is the fractional open area with respect to the total area of the porous face-sheet, t and d are the thickness of the face-sheet and the orifice diameter, respectively, and λ is the acoustic wavelength (c_0/f). $|u_0|$ represents the acoustic particle velocity through the orifices, M is the steady flow Mach number around the face-sheet, and k is an empirical constant related to the boundary layer properties of the grazing flow [28,29].

The first term on the right-hand side in Eq. (2) refers to the Helmholtz resistance for a perforated plate, which is related to viscous and mass effects [30]. The second term represents the resistance due to radiation effects [30]. The last term refers to non-linear effects, due to a high amplitude of pressure fluctuations (represented in the acoustic particle velocity) or due to steady flow tangential to the orifices in the face-sheet (represented by the free-stream Mach number) [31]. For this work, the grazing flow contribution is disregarded since, for the chosen installed jet set-up, there is no flow scrubbing on the surface, as described in mo Section 2.5. Moreover, since the goal of the liners is to dampen noise produced by the source located at the surface trailing edge, it is not necessary to account for shear layer refraction effects since the acoustic waves reach the resonators directly without propagating through the jet. The acoustic particle velocity through the orifice is given by [26]:

$$|u_0| = \frac{2|p_i|}{\sigma\rho c_0[(\theta + 1/\cos\phi)^2 + \chi^2]^{1/2}}, \tag{3}$$

where p_i and ϕ are the pressure amplitude and incidence angle of the acoustic wave on the face-sheet, respectively. For this work, it is assumed a normal incidence ($\phi = 0°$). Due to the characteristics of the main acoustic source, which is a line located at the flat plate trailing edge rather than a single point, it is likely that each region on the plate experiences sound waves with a wide range of incidence angles. Therefore, the assumption of normal incidence is a simplification to the design method given the complexity to determine the incidence accurately, which would have to be performed at localized elements on the surface, also resulting in different resonator geometries throughout the plate.

The expression for the reactance is given by [26]:

$$\chi = \frac{\sqrt{8\nu\omega}}{\sigma c_0}\left(1+\frac{t}{d}\right) + \frac{\omega(t+\delta)}{\sigma c_0} - \cot\left(\frac{\omega L_c}{c_0}\right), \tag{4}$$

where δ is the orifice end correction term and L_c is the cavity depth (distance between the face-sheet and backplate). The first and second terms on the right-hand side refer to the viscous reactance and mass inertance terms, whereas the third term is related to the impedance of the cavity [30]. The mass inertance is dependent on the parameter δ, given by [26]:

$$\delta = \frac{8}{3\pi}\frac{d(1-0.7\sqrt{\sigma})}{1+305M^3}\left(\frac{1+5\times10^3 M_0^2}{1+10^4 M_0^2}\right), \tag{5}$$

where M_0 is the acoustic particle Mach number through the orifice ($|u_0|/c_0$). The orifice end correction term takes into account interior and exterior orifice interactions, steady flow effects and high amplitude pressure fluctuations [30].

The values of resistance and reactance can be used to calculate the resonator absorption coefficient α, given by [26]:

$$\alpha = \frac{4\theta\cos\phi}{(\theta\cos\phi + 1)^2 + \chi^2\cos^2\phi}, \tag{6}$$

The goal of the design procedure is to select parameters, which result in maximum absorption at a specified frequency value. For this condition, it is thus necessary that $\alpha = 1$ and $d\alpha/d\omega = 0$, which result in $\theta = 1/\cos\phi$ and $\chi = 0$. These values are, therefore, applied in Eqs. (2) and (4), along with case-specific inputs that are necessary to solve the system of equations.

For this work, the face-sheet thickness, the number of orifices and their diameter are specified as inputs, along with the desired resonance frequency f_{res} and static fluid conditions (ambient pressure and temperature). The amplitude of the incident acoustic waves is also input. Therefore, Eq. (2) becomes an implicit relation for the fractional open area σ, which is solved numerically. Since the orifice geometry is known, the dimensions of the cavity cross-section, which is defined to be the same as the face-sheet width, is determined. The obtained value for σ is applied in Eq. (4), which allows for the calculation of the cavity depth L_c, and thus all geometric parameters of the resonator are obtained.

In order to increase the frequency range of high sound absorption by the resonator, a DDOF concept is also designed. The presence of the septum inside the cavity results in a second peak in the absorption coefficient curve, thus resulting in higher noise

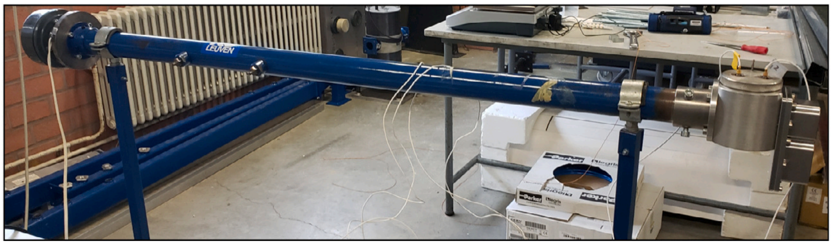

Fig. 1. Impedance tube set-up. On the left hand side of the duct there is the sound source, whereas on the right hand side there are the pressure sensors and the resonator model.

reduction in the frequency range near this additional peak [18]. For this concept, the direct application of the method proposed by Guess [26] is no longer possible due to the additional variables of the porous septum, which require further assumptions to be taken. The overall impedance of a DDOF resonator is given by [18]:

$$z = z_1 + \frac{z_2 \dfrac{\cos(kL_{c1})\sin(kL_{c2})}{\sin(kL_c)} - \mathrm{i}\cot(kL_c)}{1 + \mathrm{i}z_2 \dfrac{\sin(kL_{c1})\sin(kL_{c2})}{\sin(kL_c)}}, \tag{7}$$

where z_1 and z_2 represent the impedance of the face-sheet and septum, respectively. The parameters L_{c1} and L_{c2} are the distances between the face-sheet and septum, and between the septum and the backplate, respectively. Their summation is equivalent to the total cavity depth L_c. For simplicity, a parameter h_c is defined as the ratio between the septum position and the total cavity depth.

The face-sheet and septum impedance values consider all the resistance and reactance terms in Eqs. (2) and (4), with the exception of the cavity reactance, which is now included in Eq. (7). Therefore, with additional inputs such as the geometry of the septum orifices and its position inside the cavity, it is possible to calculate the overall impedance of the resonator. It is considered that the septum total area is equal to the cross-section of the cavity. For the initial geometry design, it is assumed that the amplitude of pressure fluctuations at the septum is equal to that of the face-sheet.

2.2. Impedance tube experiment

In order to validate the resonator concepts designed with the method from the previous section, an experiment is carried out with an impedance tube. For this work, the impedance tube at KU Leuven has been used. The set-up for the experiment is shown in Fig. 1.

The set-up consists in a steel duct of 40 mm internal diameter and 1.5 m length [32]. At one end of the duct, there is a 60 W horn driver to generate acoustic waves with a given amplitude and frequency. For this work, white noise has been generated at a given SPL. At the other end of the duct, the resonator model is attached. Two PCB-106B sensors are placed inside the duct to record pressure fluctuations. A Siemens Scadas Mobile acquisition system in combination with the Siemens Testlab software is used to generate the excitation signal and to measure the transfer function between the two microphones, which is used to compute the impedance of the resonator. Further information on the set-up can be found in Ref. [32].

The resonator impedance is determined using the two-microphone transfer-function method [33]. This technique is based on identifying the incident and reflected acoustic waves at a sample, using the transfer function measured between the two pressure sensors in the duct to determine the reflection coefficient and, consequently, the impedance of the model [33]. From this value, the resistance and reactance components, as well as the absorption coefficient can be calculated.

2.3. Flow solver

The study on JIN reduction with acoustic liners is performed via numerical simulations. Moreover, a computational impedance tube set-up is used to obtain the impedance characteristics of different resonator geometries, which are not possible to be measured in the facility previously described. The simulations are performed using the commercial software SIMULIA PowerFLOW 6-2019, which is based on LBM-VLES. This method solves the discrete form of the Boltzmann equation by explicitly tracking the development of particle distribution functions at the mesoscopic scale. The Navier–Stokes equations can be recovered through the Chapman–Enskog expansion, and fluid properties such as density, momentum and internal energy are obtained through a local integration of the particle distribution [34]. The solution of the Boltzmann equation is performed on a Cartesian mesh (lattice), with an explicit time integration and collision model.

A VLES model accounts for the unresolved scales of turbulence, with a modified two-equations $k-\epsilon$ Renormalization Group (RNG) turbulence model employed to compute a turbulent relaxation time that is added to the viscous relaxation time [35]. The relaxation time is then used to adapt the Boltzmann model to the characteristic time scales of a turbulent flow motion. Hence, the Reynolds stresses are not explicitly derived from the governing equations, but they are an implicit consequence of the chaotic

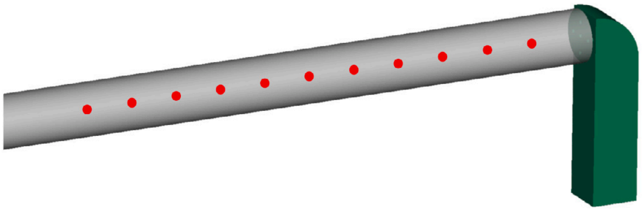

Fig. 2. Numerical set-up of an impedance tube. The duct is shown in gray, the resonator in green and the red dots are the probes where data is sampled. (For interpretation of the references to color in this figure legend, the reader is referred to the web version of this article.)

exchange of momentum driven by the turbulent flow, with characteristic times smaller than the slowly-varying turbulent flow. As such, the Reynolds stresses have a non-linear structure and are better suited to represent turbulence in a state far from equilibrium, as in the presence of distortion, shear, and rotation [36]. A wall model is also adopted to approximate the no-slip boundary conditions, which is based on an extension of the generalized law-of-the-wall model, taking into account the effect of pressure gradients [37]. A more detailed description of the flow solver can be found in Ref. [27].

For the installed jet simulations, the far-field noise is estimated through the Ffowcs-Williams and Hawkings (FWH) analogy [38], adopting the formulation 1A from Farassat extended to a convective wave equation [39,40], applied to a permeable surface encompassing the jet and plate. This approach is implemented in the time domain using a source-time dominant algorithm [41].

2.4. Impedance tube simulation

A numerical impedance tube set-up, similarly to the one described in Section 2.2, has been developed to determine the impedance of different resonator geometries, since the experimental set-up is constrained to a single duct diameter. The numerical set-up is shown in Fig. 2, with the duct, the resonator sample (shown in green) and probes to record the necessary data for impedance computation (red points). Aside from reduced costs, the advantage of a numerical set-up is that the diameter of the duct can be adapted for different face-sheet sizes, and a wider frequency range can be covered.

The simulations are carried out with an LBM-VLES solver, described in detail in Section 2.3. The input acoustic waves are generated with a broadband wave-packet model of constant amplitude in the frequency range of the analysis, simulating a white noise input with prescribed SPL and a frequency range of interest. The wavepacket is built in the time domain and imposed as initial condition of the simulation by setting the pressure and velocity values on one end of the impedance tube, which then propagate until reaching the resonator at the other end of the tube.

The length of the duct, as well as the physical simulation time are a function of the prescribed minimum frequency to be analyzed, defined as 50 Hz for all configurations. The maximum frequency of the analysis is a consequence of the duct diameter. However, for all tested cases, the threshold is significantly higher than the JIN frequency range of interest. The mesh resolution for this set-up is defined as the number of grid elements in the diameter or thickness of the orifices of the face-sheet or septum (for the DDOF case), whichever one is the smallest. In the LBM, a cartesian mesh is applied in the domain with prescribed element sizes in certain volumes known as Variable Resolution (VR) regions. As shown in Fig. 3, the minimum element size corresponds to VR8, with 15 elements for the medium resolution grid (0.13 mm element size). From there, the element size doubles as the VR number decreases. The backplate is included in VR5 (8x the element size at the orifices — approximately 1 mm), whereas the tube region upstream of the orifices is kept at VR4 (approximately 2 mm element size).

The simulation time-step is defined as the minimum grid size divided by the speed of sound. For a medium grid resolution, with 15 elements in the face-sheet orifice diameter, the obtained time-step is 2.02×10^{-7} s. The simulated time is a function of the prescribed minimum frequency of the analysis, defined as 50 Hz for the cases in this work, thus resulting in 0.02 s of physical time in the simulations. The medium resolution SDOF cases have approximately 2.58×10^{6} mesh elements and run for 1.31×10^{5} timesteps. Each case at this resolution has a computational time of 160 CPUh.

Ten probes are equidistantly placed inside the tube, upstream of the resonator, as shown in Fig. 2, which record velocity and pressure signals used to compute the impedance.

2.5. Installed jet test case

The selected test case for this work is the installed jet configuration reported by Rego et al. [27], which consists of a solid flat plate placed in the vicinity of a single-stream jet nozzle (SMC000), as shown in Fig. 4. The SMC000 is a round, convergent nozzle with an exit diameter $D_j = 50.8$ mm, used for studies on subsonic jets [3]. Two geometrical flat plate configurations are studied: length $L = 4D_j$ with height $h = 1D_j$, and $L = 6D_j$ with $h = 1.5D_j$. The length corresponds to the distance between the nozzle exit plane and the trailing edge, whereas the height is the position of the lower side of the plate with respect to the jet centerline. Previous work [27] has shown that there is no grazing flow on the surface for either of those configurations. The plate extends $1D_j$ upstream of the nozzle exit plane for the configuration with $L = 4D_j$, and $3D_j$ for the configuration with $L = 6D_j$. This is done to avoid scattering effects at the leading edge and properly account for noise shielding at shallow upstream angles. In the spanwise direction, the plate has a width of $36D_j$ to avoid side-edge scattering.

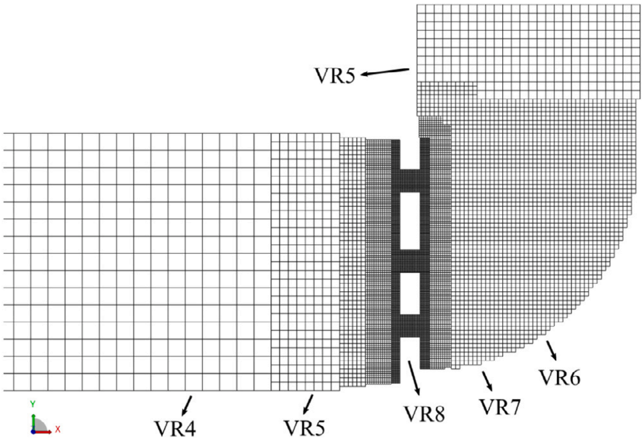

Fig. 3. Mesh refinement in the numerical impedance tube set-up. The Variable Resolution (VR) regions define the element size, which increases by a factor of 2 for each consecutive decreasing VR number.d.

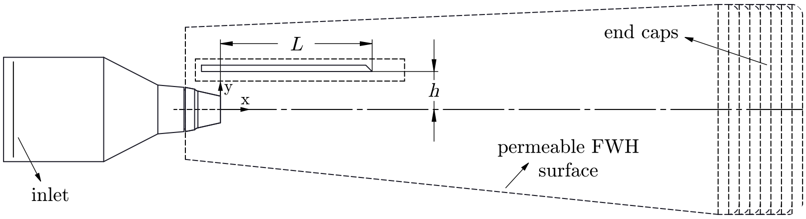

Fig. 4. Installed jet configuration with a flat plate with length L and height h, placed outside of the steady jet flow [27].

Table 1
Jet flow conditions based on Nozzle Pressure Ratio (NPR), acoustic Mach number M_a and Reynolds number Re.

Condition	NPR [−]	T_R [−]	M_a [−]	Re [10^5]
1	1.090	0.98	0.35	4.14
2	1.196	0.95	0.50	5.92

Based on the configuration in Fig. 4, an array of resonators is mounted inside the plate with the porous face-sheet on the lower side (reflected side). Therefore, the plate thickness for each case is dependent on the cavity dimensions. Different resonator sizes are applied for each geometric case since the target acoustic wave amplitude and frequency range are also case-dependent.

Two flow conditions are investigated, characterized by subsonic jets with acoustic Mach number ($M_a = U_j/c_\infty$) $M_a = 0.35$ and $M_a = 0.5$, similarly as done by Rego et al. [27]. The latter is the main one assessed in this work, and the one used for deriving the inputs for the resonator design. The former is studied in order to determine off-design results for the resonator and verify a possible degradation of the sound absorption. Jet flow properties are reported in Table 1, such as the Nozzle Pressure Ratio (NPR), the temperature ratio T_R (ratio between the jet and ambient static temperature), and the Reynolds number Re, based on the nozzle exit diameter. Static flow parameters of ambient pressure and temperature are taken from Ref. [27].

A permeable FWH surface encompasses the relevant sound sources in the set-up, as shown in Fig. 4. The far-field noise levels are computed on a microphone arc array, centered at the nozzle exit plane, with a radius of $100D_j$. Microphones are placed at an interval of 5°, ranging from $\theta = 50°$ to $\theta = 165°$ ($\theta = 180°$ corresponds to the jet axis), as shown in Fig. 5. The noise levels are evaluated at both shielded and reflected sides of the plate. Additional information on the computational set-up of the installed jet can be found in Ref. [27].

The JIN simulations with a lined plate have 3.96×10^8 mesh elements (1.08×10^8 fine equivalent elements which are updated at every time step). The finest element size (0.14 mm) is placed at the jet lipline near the nozzle to accurately capture the shear layer formation, and at the face-sheet/septum orifices. The physical time of the simulations is divided into an initial transient, consisting of 5 flow passes through the FWH surface, considering the nominal jet velocity as reference, and an acquisition time of 27 flow passes (total simulation time of 32 flow passes). The unsteady pressure on the FWH surface is sampled with a frequency of 84 kHz and 120 kHz for conditions 1 and 2, respectively. The resultant physical simulation time and acquisition parameters are shown in Table 2 for the simulated jet flow conditions. The frequency resolution refers to the minimum frequency band obtained from the FFT of the acoustic signals, based on the acquisition time and the block length and overlap applied in the signal processing. The

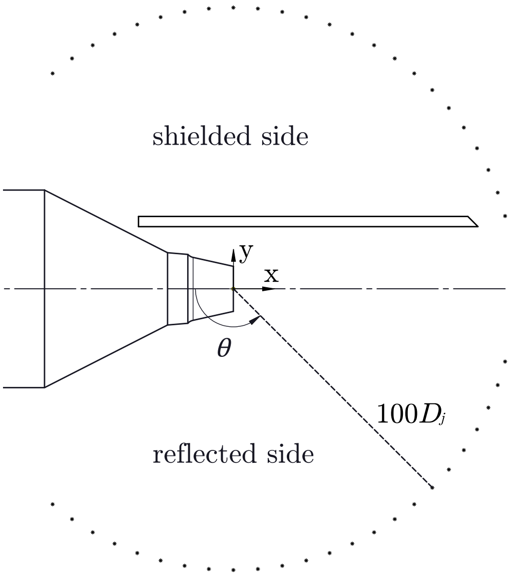

Fig. 5. Far-field microphone positions in a polar arc array, placed at the reflected and shielded sides of the jet. Microphone distance not to scale.

Table 2
Simulation physical time and acquisition parameters.

Condition	M_a [−]	Physical simulation time [s]	FWH Acquisition time [s]	Frequency resolution [Hz]
1	0.35	0.344	0.320	31
2	0.50	0.264	0.224	44

timestep is 1.5×10^{-7} s and the total number of timesteps is 1.12×10^{6}. Each installed jet simulation has a computational time of 52 kCPUh.

3. Liner design and characterization

3.1. Acoustic input parameters

In order to design a resonator for the proposed test cases, it is necessary for the acoustic characteristics of the system to be known beforehand, i.e. the desired resonance frequency and amplitude of pressure fluctuations generated by the plate. For this work, they are extracted from a previous study of an installed jet with the baseline solid surface, for which the set-up has been already validated [27]. It is assumed that the attenuation for the JIN case matches the absorption coefficient behavior of the resonator, and thus, the resonance frequency of the liner is chosen as that of the peak noise levels in the installed jet noise spectrum. The SPL spectra shown in Fig. 6 are computed from the maximum level of pressure fluctuations on the reflected side of the plate, for both geometric configurations with a $M_a = 0.5$ jet. The values are obtained for a 100 Hz frequency band and a reference pressure of 2×10^{-5} Pa is used for the conversion to dB. The peak frequency for each case is highlighted with a vertical dashed line.

Both spectra display a high amplitude, in the order of 130 dB, particularly at low frequencies (up to 1 kHz). For the $L = 4D_j$ configuration, the peak frequency is found as $f_{\text{peak}} = 700$ Hz, whereas for $L = 6D_j$ a $f_{\text{peak}} = 400$ Hz is obtained. With the longer plate, strong fluctuations are obtained at low frequencies due to increasing energy content of large scale structures when moving downstream of the nozzle exit. Moreover, the difference in amplitude between the two curves, particularly at mid and high frequencies, is linked to the radial position of the plate, the $L = 4D_j$ plate is closer to the shear layer ($h = 1D_j$) in comparison to the $L = 6D_j$ one ($h = 1.5D_j$). The resonators for each configuration are designed targeting those peak frequencies for maximum absorption.

The correct input to calculate the acoustic particle velocity in Eq. (3) is the standard deviation of the pressure time signal, equivalent to the Overall Sound Pressure Level (OASPL). This distinction is particularly important for a JIN application, which has a clear broadband characteristic, rather than tonal. The OASPL is, therefore, computed and plotted on the reflected side of the plate for the $L = 4D_j$ configuration and $M_a = 0.5$ jet, as shown in Fig. 7 in dB scale.

The amplitude of surface pressure fluctuations increases in the downstream direction, with the highest levels located near the trailing edge, at the symmetry plane of the plate ($\text{OASPL}_{\max} = 140$ dB for this configuration). This behavior is due to a combination of increased energy content of the turbulent structures in the jet downstream of the nozzle exit, and the spreading of the flow in the radial direction, resulting in a closer proximity between the plate and the turbulent structures in the jet mixing layer. A similar trend

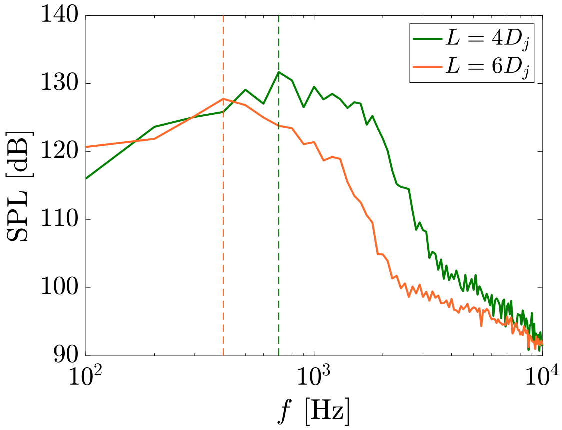

Fig. 6. Spectra of maximum SPL on the reflected side of the surface for the two plate geometries, at a $M_a = 0.5$ condition.

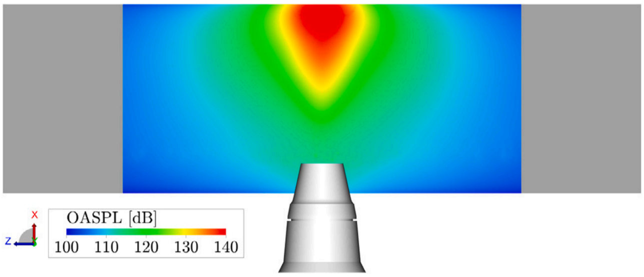

Fig. 7. OASPL on the reflected side of the plate for the installed jet configuration with $L = 4D_j$ and $h = 1D_j$, at a $M_a = 0.5$ condition.

is obtained for the $L = 6D_j$ configuration, but with an $\text{OASPL}_{\text{max}} = 135$ dB. For the design of the resonator, these $\text{OASPL}_{\text{max}}$ values are used to calculate the acoustic particle velocity in Eq. (3) and, consequently, the non-linear term in the impedance formulation.

3.2. Validation of the design approach

With the acoustic inputs in hand, it is necessary to define further constraints for the design of the resonators. The most significant one is the limited space in the y−direction due to the thickness of the plate, which is expected to be kept small. Therefore, a curved-cavity concept is selected for this application, wherein the cavity curves towards the spanwise direction of the plate. This concept is based on a folded cavity design [25]. The drawings in Fig. 8 display the SDOF concept adopted for this work, along with the main parameters of the resonator geometry.

A tridimensional and a cut view of the liner are shown in Fig. 8(a), where the face-sheet, cavity and solid backplate are identified. Unlike the concept of an L-shaped cavity proposed by Sugimoto, Murray and Astley [25], this design eliminates the vertical portion of the cavity, thus resulting in a smaller size in the direction normal to the face-sheet (direction of the plate thickness for the JIN application). There is also a curved section below the face-sheet to provide a smooth change in direction of the sound waves. The main geometric variables are shown in the drawings in Fig. 8(b). The number of orifices and dimensions t and d are selected as input, and the method outputs the cavity dimensions. For this concept, a square cavity cross-section has been selected with edge D. The cavity length is defined as the overall distance between the central orifice and the backplate, considering the one-quarter circle path and the straight section. Therefore, while the circular path is a result of the cavity height, the straight part is dimensioned to match the length provided by the design method.

It has been selected that all configurations in this work have five orifices distributed over a region on the face-sheet with edge D, with one orifice at the center and the remaining placed in an X shape and at variable distances from the central one. Preliminary simulations of the installed jet with the resonator orifices placed equidistantly have shown a strong tone in the noise spectrum. This tone occurs at a frequency corresponding to a wavelength of one-quarter of the distance between the orifices. Moreover, tones have been also shown to occur when three or more orifices are placed in a single line. Therefore, to avoid tonal noise generation by the resonators, the outer orifices are placed at different distances with respect to the central one, and their centers are not collinear.

Before calculating the dimensions of the resonators for each installed jet configuration, it is necessary to verify that the curved cavity concept has the same impedance and absorption coefficient values as those that are output from the design methodology in Section 2.1. For this purpose, the impedance of the curved cavity resonator is measured experimentally, as described in Section 2.2.

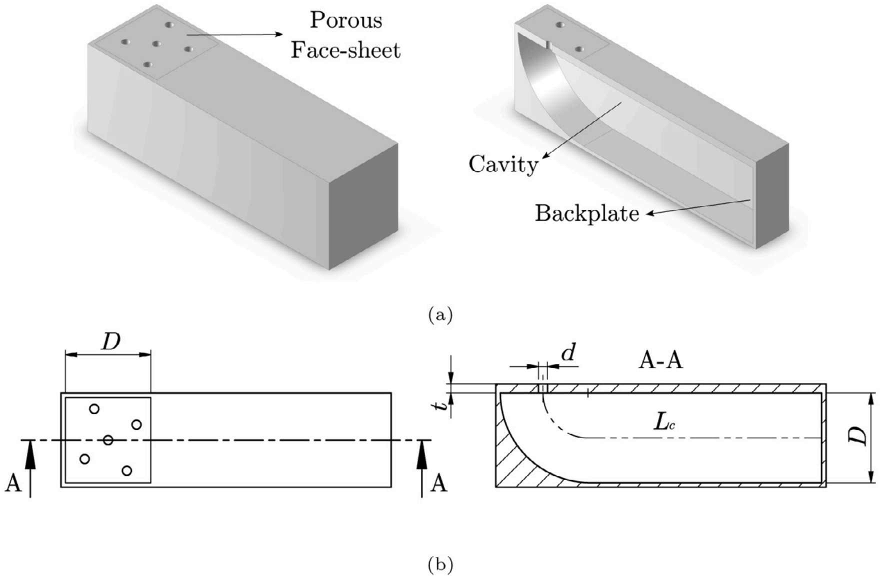

Fig. 8. (a) Tridimensional view of the curved resonator concept for JIN application. The porous face-sheet the cavity and the backplate are highlighted. (b) Top and cut views of the resonator with the main geometric parameters.

Table 3
Design parameters for the resonator used in the impedance tube experiment and validation.

Orifices	d [mm]	t [mm]	D [mm]	$D_{\text{face-sheet}}$ [mm]	L_c [mm]	f_{res} [Hz]	p_i [dB]
5	2	1	35	40	67	400	120

The results from this experiment are also used to validate the numerical impedance tube set-up, which is used to compute the properties of resonators with different dimensions.

Despite the proposed concept having a square face-sheet (and square internal cross-section), geometries with circular face-sheets with equivalent area and diameter $D_{\text{face-sheet}}$ are used in order to have the sample properly connected to the impedance tube. With the same face-sheet area, the porosity does not change with respect to design conditions. Due to the dimensions of the tube for the experiment, a concept has been especially designed for validation purposes. Moreover, the acoustic input parameters have been chosen in order to approximate those of the installed jet cases, but also following the limitations of the experimental set-up. For example, the maximum achievable OASPL for white noise input in the tube is 120 dB. The geometric parameters of the resonator used in the validation experiments are reported in Table 3. The resistance, reactance and absorption coefficient are compared to the results obtained from the design method, as well as the numerical simulations of the impedance tube, as shown in Fig. 9.

The graphs in Fig. 9 for the reactance and absorption coefficient show that a good agreement is obtained between the design methodology and both the experiment and numerical simulation of the impedance tube. On the other hand, the resistance values from the Guess method show some discrepancy, particularly at very low and very high frequencies; the agreement is better near the point of maximum absorption. However, the numerical impedance predictions agree well with the experimental results, with the trend and amplitude well captured, and thus the computational set-up is considered to be validated. Therefore, it is concluded that the proposed concept has sound absorption characteristics proper of a standard Helmholtz resonator. Moreover, the Guess method is shown to provide a good estimation for the resonator dimensions at the required conditions.

Aside from experimental validation, it is necessary to assess the grid convergence of the impedance tube numerical results. The results plotted in Fig. 9 are obtained with 20 grid elements (fine resolution) along the smallest dimension in the face-sheet channels, i.e. the thickness t, for this configuration. Therefore, to assess convergence, simulations have been carried out with 10 (coarse resolution) and 15 (medium resolution) grid elements in the channel thickness, and the impedance parameters are compared in Fig. 10. The resistance results for the coarse and medium resolutions show some oscillation at very low frequencies, although less noticeable for the latter. The reactance and absorption coefficient curves show small differences at very low frequencies as well. However, the results for the medium resolution agree well with those of the fine grid, particularly near the absorption peak, which is the region of highest interest. These results are also in qualitative agreement with an impedance characterization in a grazing flow tube, performed by Avallone et al. [42]. Therefore, to avoid high computational costs, further simulations shown in this work are performed with 15 elements in the orifice diameter.

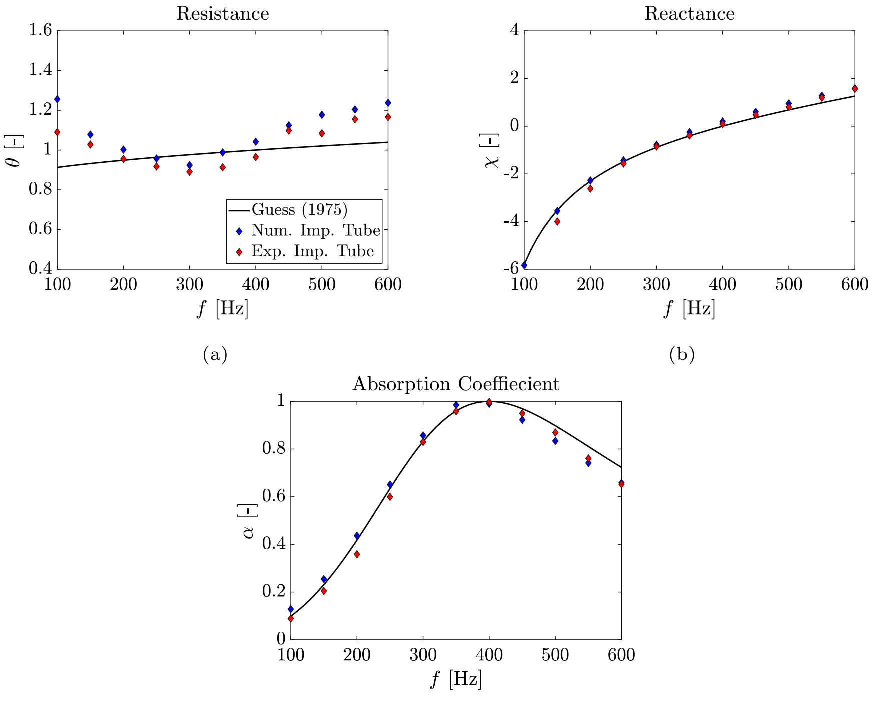

(a) (b) (c)

Fig. 9. Comparison of resonator impedance characteristics and absorption coefficient, obtained from the Guess method [26], and the impedance tube experiment and numerical simulations.

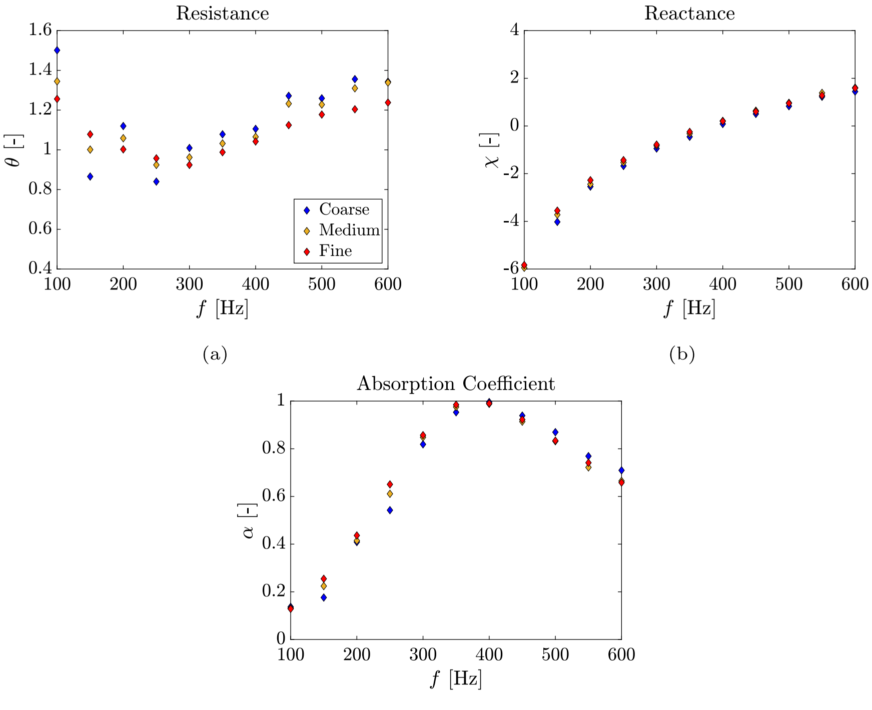

(a) (b) (c)

Fig. 10. Comparison of resonator impedance characteristics and absorption coefficient, obtained from numerical impedance tube simulations, for different grid sizes.

Table 4
Design parameters for the SDOF resonators applied in the JIN test cases.

Configuration	Orifices	d [mm]	t [mm]	D [mm]	L_c [mm]	f_{res} [Hz]	p_i [dB]
$L = 4D_j$	5	2	2	20	61	700	140
$L = 6D_j$	5	2	4	22	90	400	135

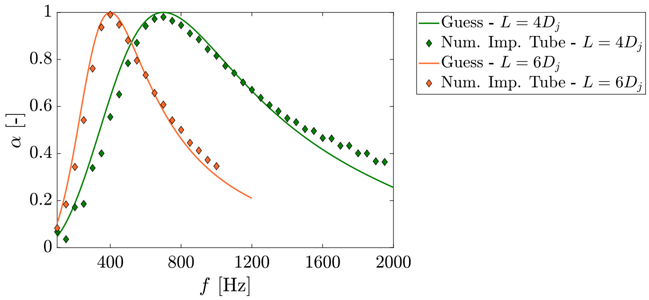

Fig. 11. Absorption coefficient for the resonators designed for the two JIN test case geometries. The lines correspond to the results obtained from the Guess method [26] and symbols are the results from the numerical impedance tube simulation.

Table 5
Design parameters for the DDOF resonators to be applied in the JIN test cases.

	$L = 4D_j$	$L = 6D_j$
Face-Sheet orifices	5	5
$d_{\text{face-sheet}}$ [mm]	2	2
$t_{\text{face-sheet}}$ [mm]	2	2
D [mm]	17	20
L_c [mm]	65	100
Septum orifices	3	3
d_{septum} [mm]	2	2
t_{septum} [mm]	4	4
h_c [−]	0.75	0.65
$p_{\text{face-sheet}}$ [dB]	140	135
p_{septum} [dB]	136	135

3.3. Liner design for JIN cases

The SDOF resonators for the installed jet test cases are designed and the absorption curves are compared to results from the numerical impedance tube. The parameters are reported in Table 4 and the absorption coefficient curve is plotted for each case in Fig. 11. The orifice thickness has been increased with respect to the validation case in order to reduce the necessary cavity length, particularly for the resonator designed for the $L = 6D_j$ configuration. This allows for more cavities to be placed inside the plate, thus potentially increasing the sound absorption. The absorption coefficient curves show a good agreement between the design methodology and the numerical impedance tube results. The peaks match the desired frequencies and only small deviations in amplitude are visible far from the peak, particularly at very high frequencies. Therefore, it is expected that the designed resonator geometries provide noise reduction when mounted in the flat plate in the vicinity of the jet.

These resonators are also used as a starting point for a DDOF design with the goal of extending the frequency range of high absorption. Since the target is to reduce a broadband region of the spectra in the installed jet configuration, the second absorption peak of the resonator needs to occur at a slightly higher frequency than the first one. This has been chosen since frequencies relatively lower to the JIN spectral peak may not be of significance in a full-scale application. Moreover, the DDOF geometrical parameters have been also constrained to provide similar absorption coefficient as the SDOF at low frequencies up to the peak. Due to the addition of the septum, and the consequent change in the overall impedance, the resonator geometry for each case has been adapted, as reported in Table 5. In the design method, the face-sheet thickness and orifice dimensions have been defined as input, based on the values from the SDOF case and adjusted manually to ensure that the absorption coefficient near the first resonance peak remains similar to the SDOF case. The impedance components are calculated using the resistance and reactance formulations in Eqs. (2) and (4), not taking into account the cavity reactance. For the septum, its size is defined to be the same as the cavity cross-section and only its position and orifice properties are changed in order to have high absorption at the desired resonance frequency (slightly above the first peak). For the non-linear term, it is assumed that the incident acoustic wave has the same amplitude as that of the face-sheet for simplification.

The absorption coefficient curves for each case are shown in Fig. 12, and compared with the respective SDOF resonator. Results are obtained from both the analytical expressions and the numerical impedance tube. The results show a good agreement between the design method and the simulations up to the first peak in the absorption coefficient curve. There is a small amplitude mismatch

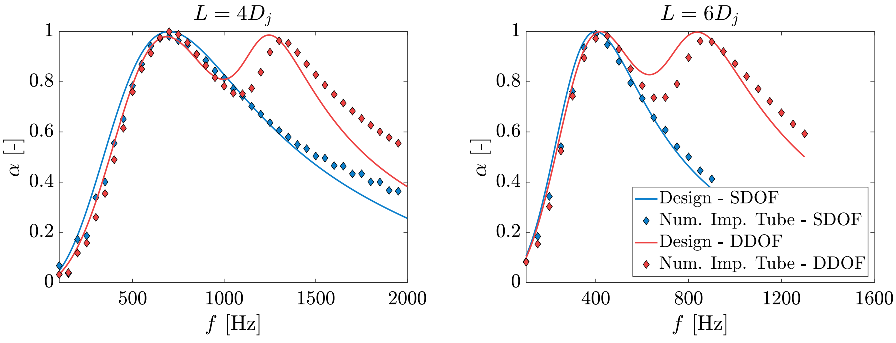

(a) (b)

Fig. 12. Absorption coefficient for the SDOF and DDOF resonators designed for the two JIN test case geometries. (a) Concept for the $L = 4D_j$ case. (b) Concept for the $L = 6D_j$ case. The lines correspond to the results obtained from the design equations and symbols are the results from the numerical impedance tube simulation.

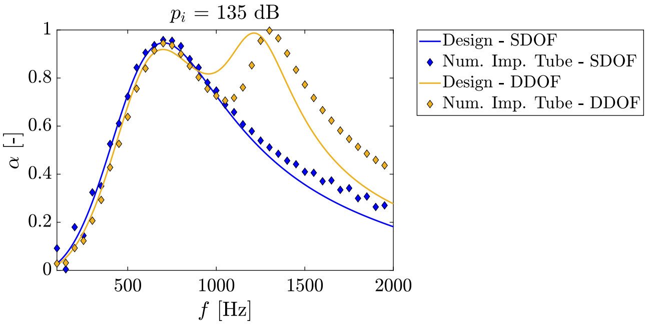

Fig. 13. Absorption coefficient for the resonators designed for the $L = 4D_j$ JIN test case with a $M_a = 0.35$ jet. The input pressure amplitude for this case is 135 dB. The lines correspond to the results obtained from the design equations and symbols are the results from the numerical impedance tube simulation.

at the valley between peaks and a deviation in the frequency of the second peak. The amplitude at the second peak, however, is reasonably predicted. With the available dataset, it is believed that the frequency shift is related to assumptions made regarding the septum. One of those is that the amplitude of incident sound waves is the same as that on the face-sheet, which may not be entirely accurate. Assumptions made by the model on the other terms of the resistance and reactance may also not be valid since the same formulation as the face-sheet has been applied. However, the difference in the second peak frequency between the design values and those of the numerical impedance tube are in the order of 50 Hz, which is acceptable for the studied application. More importantly, the results show that the DDOF concept increases the absorption characteristics of the liners at relatively higher frequencies, but still in the range of interest for the JIN test cases. Moreover, there is no significant reduction of the absorption coefficient near the first peak, with respect to the SDOF concept. There is a slight decrease in amplitude at very low frequencies, but those are not of significant interest, particularly when considering a full-scale application.

Finally, the resonators for the $L = 4D_j$ configuration are also assessed for a different jet velocity ($M_a = 0.35$), and thus at off-design conditions. A similar analysis as the one carried out in Section 3.1 has provided a maximum OASPL of 135 dB on the lower side of the plate for this flow condition, thus lower than the design value. Using this as input, the resultant absorption coefficient has been computed for the SDOF and the DDOF concepts for the $L = 4D_j$ test case, as shown in Fig. 13. For the SDOF concept, there is a reduction of the peak amplitude of approximately 6% with respect to design conditions, and thus it is expected that the liner will still perform efficiently at this condition. For the DDOF, there is a similar trend as for the previous cases regarding the agreement between the analytical expressions and the simulations. Nonetheless, similar absorption values to the SDOF are obtained near the first peak, whereas the second peak has a even higher amplitude at this condition, which is predicted by both methodologies with only a mismatch in frequency. Therefore, this concept is also expected to provide noise reduction for the JIN test cases.

Since the liners have been characterized for all cases and conditions, the next step is to locate the resonators in the plate. The arrangement consists of several rows of resonators throughout the plate length, as shown in Fig. 14. Since the test cases simulate a jet-flap interaction in an aircraft geometry, the goal is to reduce noise for an observer on the ground, i.e. at the reflected side of the plate. Therefore, the face-sheets of the resonators are located on the lower side of the surface, whereas on the upper side a solid surface is kept. The face-sheets are initially placed with the central orifice at $z = 0$, which also corresponds to the region of maximum noise production. Thereafter, the direction of the cavities alternate for each row in order to have a better distribution of the porous face-sheets throughout the surface. The number of rows is limited by the plate length of each case and the maximum

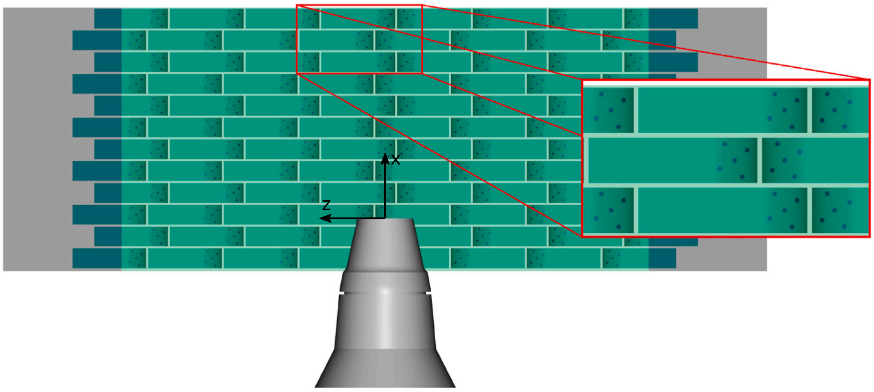

Fig. 14. Bottom view of the flat plate with rows of resonators mounted inside. Porous face-sheets are distributed throughout the surface by alternating the cavity direction for each row. (For interpretation of the references to color in this figure legend, the reader is referred to the web version of this article.)

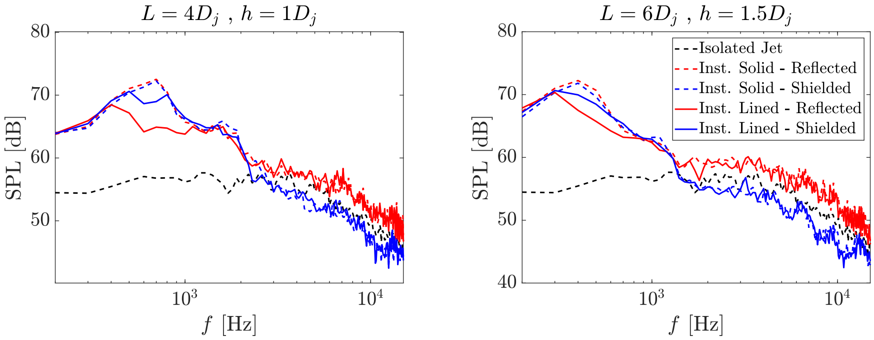

(a)

(b)

Fig. 15. Far-field spectra for the installed jet configurations, comparing the lined and solid plate results. Isolated jet noise levels are included as reference. Spectra obtained for $\theta = \pm 90°$ (reflected and shielded sides) and $M_a = 0.5$. (a) $L = 4D_j$, $h = 1D_j$. (b) $L = 6D_j$, $h = 1.5D_j$.

span to place a face-sheet has been limited to $10D_j$, which also corresponds to the data sampling region on the plate (represented by the light green region in Fig. 14).

4. Jet-installation noise with a lined plate

4.1. Far-field results

In this section, the results from the simulations of the installed jet with the lined plates are compared to the baseline solid case. SPL spectra are plotted in Fig. 15 for the two geometric cases. The spectra are obtained for a constant frequency band of 100 Hz, at polar angles $\theta = \pm 90°$ (reflected and shielded sides).

The lined plate provides significant noise reduction with respect to the baseline solid configuration, particularly for the observer at the reflected side ($\theta = 90°$). For the $L = 4D_j$, $h = 1D_j$ case, shown in Fig. 15(a), a reduction of 7.5 dB is obtained at 700 Hz, which is the design resonance frequency of the cavity. Moreover, the SPL is visibly lower in the range 400 Hz $< f <$ 1100 Hz, for which $\alpha > 0.7$, according to the plot in Fig. 11. No noise reduction is visible at higher frequencies, for which turbulence mixing noise reflected on the plate is the dominant mechanism. A similar behavior occurs for the $L = 6D_j$, $h = 1.5D_j$ case with a reduction of 5 dB at the resonance frequency ($f_{\text{res}} = 400$ Hz) for the reflected side observer. Noise abatement for this case occurs for 300 Hz $< f <$ 700 Hz, which shows that the liner performs better at frequencies higher than the absorption peak, in agreement with the absorption coefficient curve.

An interesting result is obtained for the observer at the shielded side ($\theta = -90°$). Although the face-sheets are present only on the lower side of the plate, a small noise reduction occurs near the resonance frequency of the resonator, in the order of 3 dB and 1.8 dB for the $L = 4D_j$ and $L = 6D_j$ configurations, respectively. Since there can be no acoustic absorption on the upper side of the plate, as there are no perforations there, it is concluded that the presence of the resonators also changes the source characteristics, prior to the scattering phenomenon. However, given the differences in SPL for observers at different sides of the lined plate, the

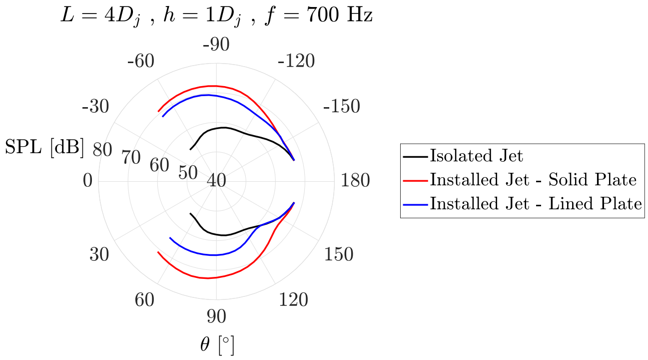

Fig. 16. SPL directivity curves of the isolated and installed jets with solid and lined plates, for a frequency $f = 700$ Hz. The installed configuration corresponds to the $L = 4D_j$, $h = 1D_j$ case, at $M_a = 0.5$.

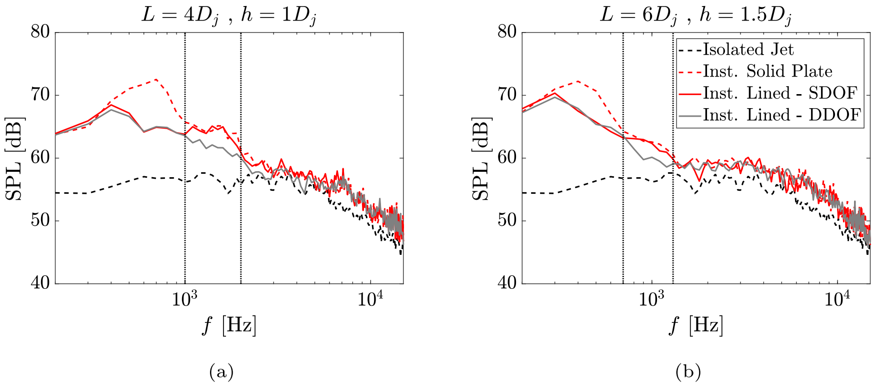

(a)

(b)

Fig. 17. Far-field spectra for the installed jet configurations, comparing the SDOF and DDOF lined configurations. Noise levels of the isolated and installed jets with solid plate are included as reference. Spectra obtained for $\theta = 90°$ (reflected side) and $M_a = 0.5$. (a) $L = 4D_j$, $h = 1D_j$. (b) $L = 6D_j$, $h = 1.5D_j$.

noise reduction obtained at the reflected side is still predominantly due to the acoustic absorption by the resonators. This is also visible in the directivity curves in Fig. 16, for the $L = 4D_j$ case.

The results show that the lined plate provides significant noise reduction (around 7 dB) for polar angles at the reflected side up to $\theta = 150°$. At shallow downstream angles, where turbulence-mixing noise becomes dominant, the curve collapses with that of the isolated jet at $\theta \geq 130°$ for the lined case, whereas for the solid one this happens only at $\theta \geq 160°$. At the shielded side, the lined plate generates noise approximately 2–3 dB lower than the baseline solid case, up to $\theta = -140°$. Therefore, it is shown that the liner provides noise reduction at all angles where installation effects are dominant. Moreover, the noise reduction for most angles on the shielded side indeed points to a change in the source properties, whose underlying mechanisms are addressed in Section 4.2.

Having obtained successful results with the SDOF liner, the next step is to assess the noise reduction capabilities of the DDOF concept. The spectra of the installed jet with a DDOF lined plate are also computed and compared with the SDOF configuration, as shown in Fig. 17 for the two installed jet geometries. The results are plotted only for the reflected side since no visible differences between the SDOF and DDOF configurations have been found for the shielded one.

The spectra for both installed jet geometries display the same trend: at low frequencies the SDOF and DDOF lined plate cases provide the same noise levels, but at mid frequencies the latter outperforms the former. For the $L = 4D_j$ case, for example, the DDOF provides an additional noise reduction of 3 dB at $f = 1400$ Hz. The frequency range where the DDOF liner provides additional noise reduction with respect to the SDOF one has been marked with dotted lines. For both cases, this region is approximately centered around the second peak in the resonator absorption curve, as shown in Fig. 12. For $L = 4D_j$, this corresponds to 1000 Hz $< f <$ 2000 Hz, whereas for $L = 6D_j$, it is 700 Hz $< f <$ 1300 Hz. Therefore, the DDOF resonator concept is capable of even further JIN reduction.

Finally, the noise levels of the lined plate configuration are assessed for the $M_a = 0.35$ jet condition. The SPL spectra for both SDOF and DDOF cases are plotted and compared to the reference solid case, as shown in Fig. 18(a), for $\theta = 90°$ (reflected side). The results show that the liners still provide significant noise abatement at this condition, with a 6 dB reduction at $f = 700$ Hz with the SDOF concept relative to the solid case, and visible difference up to $f = 1000$ Hz. Moreover, the DDOF concept shows the same trend as for $M_a = 0.5$ with an additional 3 dB reduction for 1000 Hz $< f <$ 2000 Hz with respect to the SDOF. This shows that the lined plate can still provide significant JIN reduction even at an off-design condition.

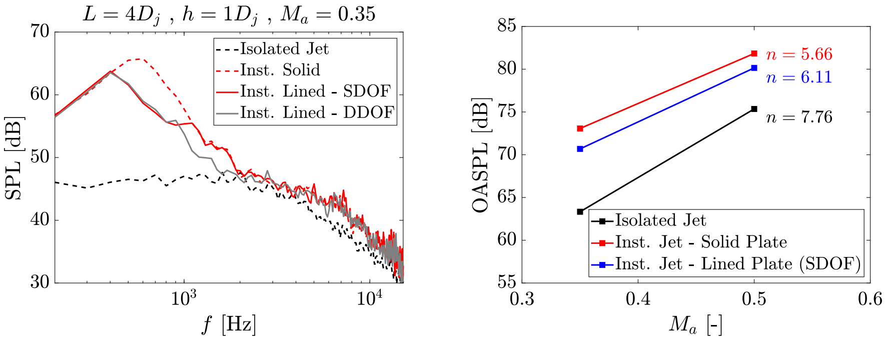

(a) (b)

Fig. 18. (a) Spectra of the installed jet configuration for lined (SDOF and DDOF) and solid plates at $M_a = 0.35$, obtained for a configuration $L = 4D_j$, $h = 1D_j$. Noise levels of the respective isolated jet are plotted as reference. Spectra obtained for $\theta = 90°$ (reflected side). (b) Overall Sound Pressure Level (OASPL) dependence on the jet acoustic Mach number for isolated and installed cases with solid and lined plates.

The dependence of the OASPL with the jet velocity is plotted in Fig. 18(b) for the solid and lined (SDOF) installed jet cases, as well as the isolated jet, considering an observer at $\theta = 90°$. The results for the DDOF case are similar to the SDOF one and thus have been omitted. The exponent n for the jet velocity is retrieved for each case and also shown in the figure. The isolated jet noise is shown to vary with $U_j^{7.76}$, which characterizes turbulence-mixing noise [43]. The installed jet with the solid plate has a dependence of $U_j^{5.66}$, which is characteristic of edge scattering [5]. Finally, with the lined plate, the noise is proportional to $U_j^{6.11}$, thus showing a decrease in the dominance of the scattering mechanism in the overall noise production.

4.2. Surface pressure fluctuations

The far-field spectra have shown that the designed liner concepts in this work are effective in reducing JIN. However, results for an observer at the shielded side of the plate indicate that the resonators are not only dampening the acoustic waves scattered at the trailing edge, which is their expected working mechanism, but also effectively changing the source properties. In order to verify this, the near-field pressure fluctuations on the upper and lower sides of the plate are analyzed. The pressure autospectrum ($\hat{P}(f)$) on both sides of the plate is plotted in logarithmic scale for different streamwise positions at the $z = 0$ plane, for the $L = 4D_j$, $h = 1D_j$ configuration, and for two different frequencies ($f = 700$ Hz and $f = 800$ Hz), as shown in Fig. 19. These frequencies have been chosen since, for the former, the liners provide noise reduction on both sides of the plate according to the far-field spectra, whereas for the latter, this occurs only on the reflected side.

On the lower side of the plate, for $f = 700$ Hz, three streamwise regions on the plate can be distinguished based on the trend between the lined and solid plates. In the upstream part of the plate (region 1), there is a significant difference between the pressure amplitudes of the lined and solid plates. This is attributed to the dampening of scattered acoustic waves, traveling upstream from the plate trailing edge, by the resonators throughout the surface. Thereafter, the curves collapse in what is defined as region 2, where it is believed that pressure waves from the jet impinging on the plate are stronger and thus mask the acoustic waves scattered at the trailing edge. Finally at region 3, near the trailing edge, the lined plate has a smaller amplitude of fluctuations with respect to the solid one, indicating that part of the impinging waves from the jet are being dampened prior to scattering. For $f = 800$ Hz, regions 1 and 2 can be clearly distinguished, but there is no significant difference between the amplitude of curves near the trailing edge. Although the curve of the lined plate is slightly lower, this difference is possibly not significant in order to affect the far-field noise.

Therefore, it is believed that near the plate trailing edge, the resonators are dampening the acoustic waves generated by the jet itself, before they are scattered, thus reducing the overall source intensity. Moreover, the liners act to reduce the surface impedance, particularly at the resonance frequency, which in turn leads to a less abrupt discontinuity at the trailing edge. As a result, the scattering mechanism also becomes weaker. The pressure fluctuations on the upper side of the plate also contribute to this conclusion since for $f = 700$ Hz there is a constant offset between the curves, likely due to a weakening of the acoustic source, whereas for $f = 800$ Hz, only small differences occur locally near the trailing edge, which do not seem to affect the remainder of the upper surface, thus also not affecting the far-field noise. It is also believed that this effect on the lower side is more pronounced near the trailing edge because the amplitude of pressure fluctuations at that region match more closely the design conditions of the resonator, in this case the p_i parameter. It is not yet clear, however, why this effect is restricted to such a narrow frequency range around the absorption peak. It is believed that this is due to the characteristics of the incident waves from the jet, which only closely match the design conditions of the resonators at this frequency range. Further research into this hypothesis is necessary.

5. Conclusions

A curved Helmholtz resonator concept is studied for reducing jet-installation noise in a configuration comprised by a single-stream subsonic jet and a nearby flat plate. The main goal of this work is to assess the noise reduction provided by the resonators, targeting the acoustic waves produced by scattering at the plate trailing edge.

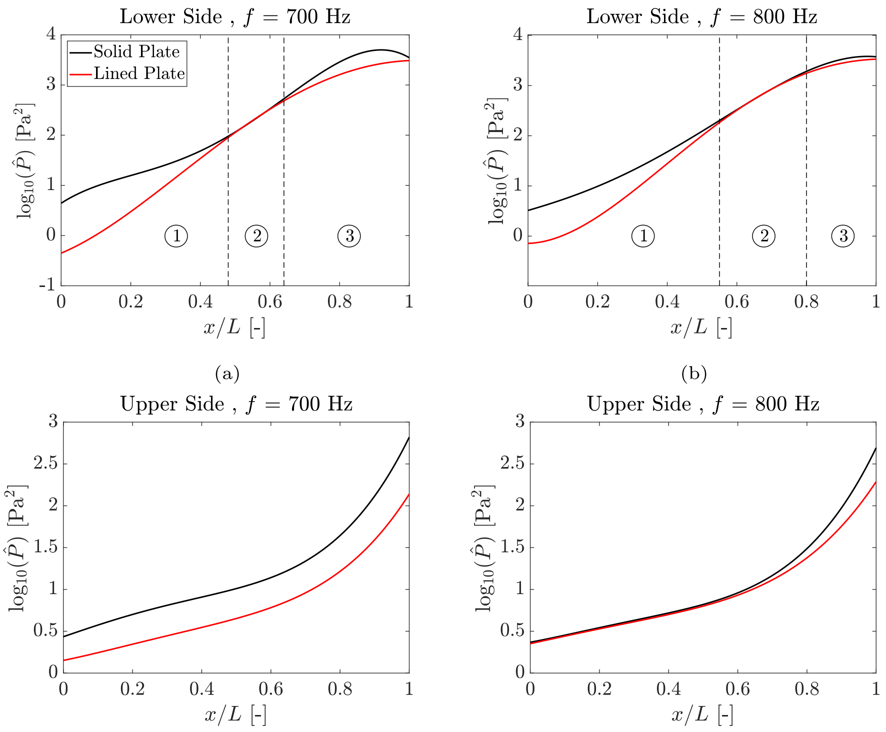

(a) (b)

(c) (d)

Fig. 19. Amplitude of pressure fluctuations ($\hat{P}$) in the streamwise direction on the lower and upper sides of the plate, at the $z = 0$ plane, at frequencies $f = 700$ Hz and $f = 800$ Hz. Results obtained for the installed jet with solid and SDOF lined plates and configuration $L = 4D_j$, $h = 1D_j$.

The Guess method [26] is applied to obtain the cavity dimensions, whereas the orifice parameters are defined as input. The amplitude of the incident pressure waves and the desired resonance frequency, which are part of the impedance formulation, are obtained from simulations of the installed jet with a fully solid plate (baseline case). The former is taken from the surface pressure fluctuations on the lower side, whereas the latter corresponds to the peak frequency in the spectrum of the installed jet configuration. Both single and double degree-of-freedom liners are studied, for which the latter contains a porous septum inside the cavity in order to expand the frequency range of high sound attenuation.

The cavity curvature is necessary in order to keep the plate thickness small. Therefore, in order to validate the design and verify that the curvature does not affect the properties of the resonator, an experiment with an impedance tube has been performed to measure the liner impedance. A good agreement has been obtained, particularly at frequencies close to the absorption peak. Numerical simulations of an impedance tube have been also performed in order to characterize resonators with different dimensions, particularly for the application in the different JIN test cases and flow conditions. The simulation results are also validated against the experiment. For the DDOF resonators, the first peak in the absorption coefficient curve is well predicted by the design methodology, but the small differences occur near the second peak. This is not a significant issue, however, since the desired trends are still visible in the impedance tube simulation results.

In the installed jet set-up, an array of resonators is placed inside the plate with the face-sheet on the lower side (reflected side). Far-field spectra show that noise reduction in the order of 7 dB is obtained at the resonance frequency for the SDOF lined plate configuration with respect to the solid plate configuration. Moreover, the lined plate has lower sound pressure levels in a broad frequency range around the resonance, thus significantly reducing the installation noise. Directivity plots show that this noise mitigation occurs for all polar angles where installation effects are dominant over turbulence-mixing. For the configuration with the DDOF resonator, further noise reduction (approximately 3 dB) is obtained at mid frequencies, which correspond to the second peak in the absorption coefficient curve. Therefore, the DDOF liner outperforms the SDOF one by expanding the frequency range of noise reduction. Simulations at an off-design condition (lower jet Mach number and consequently, lower amplitude of incident wave) show that the liners are still effective in reducing noise. By computing the dependence of the overall sound pressure level with the jet velocity, it is shown that the trailing-edge source becomes less dominant with respect to turbulence-mixing noise for the liner plate.

Finally, the results also show that a slight noise reduction also occurs on the shielded side of the plate, but at a significantly narrower band around the resonance frequency. The SPL amplitude is also higher than that on the reflected side. Computations of the surface pressure fluctuations show three distinct regions by comparing the solid and lined plates. At the resonance frequency, near the leading edge the amplitude of fluctuations on the lined plate is significantly lower than the baseline, which is due to the attenuation of the scattered waves traveling upstream from the trailing edge. A second region is visible where the curves collapse, where fluctuations of hydrodynamic characteristic are likely dominant. Finally, near the trailing edge, again the lined plate has a lower amplitude of fluctuations than the baseline. This is believed to be the result of the absorption of acoustic waves from the jet itself prior to their scattering at the trailing edge, and a less abrupt impedance discontinuity at the trailing edge. Consequently, this reduces the overall trailing-edge source strength, which also affects the noise propagated at the reflected side. This effect is, however, not visible outside of the resonance frequency, which explains the reason for the narrow frequency range where noise reduction is obtained at the shielded side.

Therefore, it is concluded that acoustic liners with curved cavities are suitable noise reduction solutions for jet-installation noise, which is inherently broadband and of high amplitude. Further research on this topic includes an analysis with the resonators mounted in an actual flap geometry, where its effects on the lift and drag forces can be estimated. Moreover, a combination of open-cell permeable materials and Helmholtz resonators can also be interesting, for which the former provides noise reduction due to flow communication between the two sides of the surface and the resonators are used to reduce the sound produced at the solid-permeable junction.

CRediT authorship contribution statement

Leandro Rego: Conceptualization, Methodology, Validation, Formal analysis, Investigation, Data curation, Writing – original draft, Writing – review & editing, Visualization. **Francesco Avallone:** Writing – review & editing, Visualization, Supervision. **Daniele Ragni:** Writing – review & editing, Visualization, Supervision. **Damiano Casalino:** Methodology, Writing – review & editing, Visualization, Supervision. **Hervé Denayer:** Validation, Data curation, Writing – review & editing, Visualization, Supervision.

Declaration of competing interest

The authors declare that they have no known competing financial interests or personal relationships that could have appeared to influence the work reported in this paper.

Acknowledgments

This work is part of the IPER-MAN project (Innovative PERmeable Materials for Airfoil Noise Reduction), project number 15452, funded by the Netherlands Organization for Scientific Research (NWO). The authors would like to thank Dr. Mirjam Snellen and Prof. Sybrand van der Zwaag from the Delft University of Technology, for collaboration in the project.

References

[1] D.L. Huff, Noise Reduction Technologies for Turbofan Engines, NASA/TM—2007-214495, 2007, pp. 1–17.
[2] J.L.T. Lawrence, M. Azarpeyvand, R.H. Self, Interaction between a flat plate and a circular subsonic jet, in: 17th AIAA/CEAS Aeroacoustics Conference, Portland, OR, USA, 2011, http://dx.doi.org/10.2514/6.2011-2745.
[3] C. Brown, Jet-surface interaction test: Far-field noise results, in: Proceedings of the ASME Turbo Expo 2012: Power for Land, Sea and Air, Copenhagen, Denmark, 2012, pp. 1–13.
[4] A.V.G. Cavalieri, P. Jordan, W.R. Wolf, Y. Gervais, Scattering of wavepackets by a flat plate in the vicinity of a turbulent jet, J. Sound Vib. 333 (24) (2014) 6516–6531, http://dx.doi.org/10.1016/j.jsv.2014.07.029.
[5] J.E. Ffowcs-Williams, L.H. Hall, Aerodynamic sound generation by turbulent flow in the vicinity of a scattering half plane, J. Fluid Mech. 40 (4) (1970) 657–670, http://dx.doi.org/10.1017/S0022112070000368.
[6] R.W. Head, M.J. Fisher, Jet/surface interaction noise: - analysis of farfield low frequency augmentations of jet noise due to the presence of a solid shield, in: 3rd AIAA Aeroacoustics Conference, Palo Alto, CA, USA, 1976, http://dx.doi.org/10.2514/6.1976-502.
[7] L. Rego, F. Avallone, D. Ragni, D. Casalino, Noise amplification effects due to jet-surface interaction, in: AIAA Scitech 2019 Forum, San Diego, CA, USA, 2019, http://dx.doi.org/10.2514/6.2019-0001.
[8] D. Papamoschou, Prediction of jet noise shielding, in: 48th AIAA Aerospace Sciences Meeting Including the New Horizons Forum and Aerospace Exposition, Orlando, FL, USA, 2010, http://dx.doi.org/10.2514/6.2010-653.
[9] D. Casalino, A. Hazir, Lattice Boltzmann based aeroacoustic simulation of turbofan noise installation effects, in: 23rd International Congress on Sound & Vibration, Athens, Greece, 2014, pp. 1–8.
[10] C. Hughes, The promise and challenges of ultra high bypass ratio engine technology and integration, in: AIAA Aerospace Sciences Meeting, Orlando, FL, USA, 2011.
[11] L. Rego, D. Ragni, F. Avallone, D. Casalino, R. Zamponi, C. Schram, Jet-installation noise reduction with flow-permeable materials, J. Sound Vib. 498 (2021) 115959, http://dx.doi.org/10.1016/j.jsv.2021.115959.
[12] L. Rego, F. Avallone, D. Ragni, D. Casalino, On the mechanisms of jet-installation noise reduction with flow-permeable trailing edges, J. Sound Vib. 520 (2022) http://dx.doi.org/10.1016/j.jsv.2021.116582.
[13] E. Sarradj, T. Geyer, Noise generation by porous airfoils, in: 13th AIAA/CEAS Aeroacoustics Conference, Rome, Italy, 2007, http://dx.doi.org/10.2514/6.2007-3719.
[14] T. Geyer, E. Sarradj, Trailing edge noise of partially porous airfoils, in: 20th AIAA/CEAS Aeroacoustics Conference, Atlanta, GA, USA, 2014, http://dx.doi.org/10.2514/6.2014-3039.
[15] J.D. Eldredge, A.P. Dowling, The absorption of axial acoustic waves by a perforated liner with bias flow, J. Fluid Mech. (485) (2003) 307–335, http://dx.doi.org/10.1017/S0022112003004518.
[16] C.K. Tam, K.A. Kurbatskii, Microfluid dynamics and acoustics of resonant liners, AIAA J. 38 (8) (2000) 1331–1339, http://dx.doi.org/10.2514/2.1132.
[17] D. Casalino, F. Diozzi, R. Sannino, A. Paonessa, Aircraft noise reduction technologies: A bibliographic review, Aerosp. Sci. Technol. 12 (1) (2008) 1–17, http://dx.doi.org/10.1016/j.ast.2007.10.004.

[18] H.H. Hubbard, Aeroacoustics of Flight Vehicles: Theory and Practice Vol. 2: Noise Control, Vol. 2, NASA Reference Publication 1258, 1991, pp. 165–206.

[19] D. Casalino, M. Barbarino, Optimization of a single-slotted lined flap for wing trailing-edge noise reduction, J. Aircr. 49 (4) (2012) http://dx.doi.org/10.2514/1.C031561.

[20] C. Teruna, F. Manegar, F. Avallone, D. Casalino, D. Ragni, A. Rubio-Carpio, T. Carolus, Numerical analysis of metal-foam application for trailing edge noise reduction, in: 25th AIAA/CEAS Aeroacoustics Conference, Delft, The Netherlands, 2019.

[21] L.J. Ayton, Acoustic scattering by a finite rigid plate with a poroelastic extension, J. Fluid Mech. 791 (2016) 414–438, http://dx.doi.org/10.1017/jfm.2016.59.

[22] M.G. Jones, W.R. Watson, D.M. Nark, B.M. Howerton, Evaluation of variable-depth liner configurations for increased broadband noise reduction, in: 21st AIAA/CEAS Aeroacoustics Conference, 2015, http://dx.doi.org/10.2514/6.2015-2697.

[23] D.T. Sawdy, R.J. Beckemeyer, Bandwidth attenuation with a folded cavity liner in a circular flow duct, AIAA J. 18 (7) (1980) 766–773, http://dx.doi.org/10.2514/3.50818.

[24] J. Yu, E. Chien, Folding cavity acoustic liner for combustion noise reduction, in: 12th AIAA/CEAS Aeroacoustics Conference, Cambridge, MA, USA, 2006.

[25] R. Sugimoto, P. Murray, R.J. Astley, Folded cavity liners for turbofan engine intakes, in: 18th AIAA/CEAS Aeroacoustics Conference (33rd AIAA Aeroacoustics Conference), American Institute of Aeronautics and Astronautics Inc., 2012, http://dx.doi.org/10.2514/6.2012-2291.

[26] A.W. Guess, Calculation of perforated plate liner parameters from specified acoustic resistance and reactance, J. Sound Vib. 40 (I) (1975) 119–137.

[27] L. Rego, F. Avallone, D. Ragni, D. Casalino, Jet-installation noise and near-field characteristics of jet-surface interaction, J. Fluid Mech. 895 (2020) http://dx.doi.org/10.1017/jfm.2020.294.

[28] E. Feder, L.W. Dean, Analytical and Experimental Studies for Predicting Noise Attenuation in Acoustically Treated Ducts for Turbofan Engines, Tech. Rep, NASA CR-1373, 1969, URL https://ntrs.nasa.gov/search.jsp?R=19690027596.

[29] E. Rice, A Model for the Pressure Excitation Spectrum and Acoustic Impedance of Sound Absorbers in the Presence of Grazing Flow, American Institute of Aeronautics and Astronautics (AIAA), 1973, http://dx.doi.org/10.2514/6.1973-995.

[30] U. Ingard, On the theory and design of acoustic resonators, J. Acoust. Soc. Am. 25 (6) (1953) 1037–1062, http://dx.doi.org/10.1121/1.1907235.

[31] U. Ingard, H. Ising, Acoustic nonlinearity of an orifice, J. Acoust. Soc. Am. 42 (1) (1967) 6–17, http://dx.doi.org/10.1121/1.1910576.

[32] R. Boonen, P. Sas, W. Desmet, W. Lauriks, G. Vermeir, Calibration of the two microphone transfer function method with hard wall impedance measurements at different reference sections, Mech. Syst. Signal Process. 23 (5) (2009) 1662–1671, http://dx.doi.org/10.1016/j.ymssp.2008.12.001.

[33] ISO-10534-2, Determination of Sound Absorption Coefficient and Impedance in Impedance Tubes, Tech. Rep., International Organisation for Standardization, Genève, Switzerland, 1998.

[34] S. Succi, the Lattice Boltzmann Equation for Fluid Dynamics and beyond, Oxford University Press, New York, NY, USA, 2001.

[35] V. Yakhot, S.A. Orszag, Renormalization group analysis of turbulence. I. Basic theory, J. Sci. Comput. 1 (1) (1986) 3–51, http://dx.doi.org/10.1007/BF01061452.

[36] H. Chen, S.A. Orszag, I. Staroselsky, S. Succi, Expanded analogy between Boltzmann kinetic theory of fluids and turbulence, J. Fluid Mech. 519 (2004) 301–314, http://dx.doi.org/10.1017/S0022112004001211.

[37] B.E. Launder, D.B. Spalding, The numerical computation of turbulent flows, Comput. Methods Appl. Mech. Eng. 3 3 (2) (1974) 269–289.

[38] J.E. Ffowcs-Williams, D.L. Hawkings, Sound generation by turbulence and surfaces in arbitrary motion, Phil. Trans. R. Soc. A 264 (1151) (1969) 321–342, http://dx.doi.org/10.1098/rsta.1969.0031.

[39] G. Brès, F. Pérot, D. Freed, A ffowcs Williams - Hawkings solver for lattice-Boltzmann based computational aeroacoustics, in: 16th AIAA/CEAS Aeroacoustics Conference, Stockholm, Sweden, 2010, http://dx.doi.org/10.2514/6.2010-3711.

[40] F. Farassat, G.P. Succi, A review of propeller discrete frequency noise prediction technology with emphasis on two current methods for time domain calculations, J. Sound Vib. 71 (3) (1980) 399–419, http://dx.doi.org/10.1016/0022-460X(80)90422-8.

[41] D. Casalino, An advanced time approach for acoustic analogy predictions, J. Sound Vib. 261 (4) (2003) 583–612, http://dx.doi.org/10.1016/S0022-460X(02)00986-0.

[42] F. Avallone, P. Manjunath, D. Ragni, D. Casalino, Lattice-Boltzmann very large eddy simulation of a multi-orifice acoustic liner with turbulent grazing flow, in: 25th AIAA/CEAS Aeroacoustics Conference, American Institute of Aeronautics and Astronautics, Reston, Virginia, 2019, http://dx.doi.org/10.2514/6.2019-2542.

[43] M.J. Lighthill, On sound generated aerodynamically I. General theory, Proc. R. Soc. A 211 (1107) (1952) 564–587, http://dx.doi.org/10.1098/rspa.1952.0060.